SAND2022-15991C

WM2023 Conference, February 26 – March 2, 2023, Phoenix, Arizona, USA

Impact of Simulated Radionuclide Release Location on Culebra Transport for WIPP PA Calculations– 23364

James Bethune*, Sarah Brunell**, and Seth King**
* Piru Associates
**Sandia National Laboratories

ABSTRACT

The Waste Isolation Pilot Plant (WIPP) has been developed by the U.S. Department of Energy (DOE) for the geologic disposal of defense-generated transuranic (TRU) waste. Containment of TRU waste at the WIPP is regulated by the U.S. Environmental Protection Agency (EPA) according to the regulations set forth in Title 40 of the Code of Federal Regulations (CFR), Part 191. As currently designed, WIPP includes ten excavated panels for the placement of waste. The DOE is looking at options to potentially excavate additional panels for waste disposal.

The DOE must demonstrate that the WIPP facility complies with the containment requirements in Title 40 CFR Part 191 by means of performance assessment (PA) calculations. WIPP PA calculations include a transient, dual-porosity mass transport model of radionuclides released into the Culebra, a dolomite that is the most transmissive unit above the WIPP excavations. Culebra transport calculations are made with calibrated steady-state flow fields, which are locally modified to account for scenarios of mining-induced subsidence and climate change. The transport simulations assume parallel plate fracturing where fluid flow is restricted to the fracture domain, mass is transferred between the fracture and matrix domains via molecular diffusion, and retardation is restricted to the matrix domain. In each transport simulation, 1 kg of each of Am-241, Pu-239, Th-230, and U-234 is released into a discrete source (release point) over the first 50 years of the simulation. The transport output of interest for PA is the cumulative mass discharge of each simulated radionuclide at the WIPP Land Withdrawal Act Boundary (LWB) in 50-year increments over the 10,000-year regulatory period.

A PA has been executed by Sandia National Laboratories for a 19-panel WIPP repository layout option. The 19-panel design is contained within the LWB, and the waste inventory used is limited to the volume of waste specified in the Land Withdrawal Act and in the Consultation and Cooperation agreement with the State of New Mexico. This work documents the impacts of the changes made to accommodate the additional panels region on the Culebra transport calculations. It describes how additional mass release points were located to capture variable flow and transport pathways emanating from point locations across the WIPP repository footprint, present the cumulative radionuclide mass transport to the LWB, and describe how the model sensitivity varies by release point and mining scenario.

Radionuclide transport simulations show that mass released above the western-most repository panels reaches the LWB significantly earlier and achieves significantly higher mass breakthrough over the regulatory period. Conservative particle tracking calculations show that mining within the LWB draws flow from over the western panels toward the western extent of the LWB. Higher mass breakthrough is associated with lower matrix distribution coefficients and with groundwater flow fields with faster particle travel times to the LWB. The matrix distribution coefficient is the most impactful control on mass transport to the LWB across all simulated scenarios and isotopes; however, groundwater flow velocity fields become increasingly impactful for simulations with mass release into the western region of the additional panels area.

INTRODUCTION

The Waste Isolation Pilot Plant (WIPP), located in southeastern New Mexico, has been developed by the U.S. Department of Energy (DOE) for the geologic (deep underground) disposal of defense-generated transuranic (TRU) waste. Containment of TRU waste at the WIPP is regulated by the U.S. Environmental Protection Agency (EPA) according to the regulations set forth in Title 40 of the Code of Federal Regulations (CFR), Part 191.

As currently certified, WIPP includes ten excavated panels for the placement of waste. For operational reasons, not all the volume of the ten excavated panels will be used for waste disposal. The DOE plans to excavate two panels, termed replacement panels, to replace lost disposal capability as certified and may consider excavating up to seven panels beyond the two replacement panels, collectively defined here as additional panels, to the northwest of the existing waste region.

The DOE demonstrates compliance with the containment requirements according to the Certification Criteria in Title 40 CFR Part 194 by means of performance assessment (PA) calculations performed by Sandia National Laboratories (SNL). WIPP PA calculations estimate the probability and consequence of potential radionuclide releases from the repository to the accessible environment for a regulatory period of 10,000 years after facility closure. WIPP PA models are used to support the repository recertification process that occurs at five-year intervals following the receipt of the first waste shipment at the site in 1999.

The Culebra Dolomite Member of the Rustler Formation has been identified as the most transmissive saturated unit above the Salado Formation and consequently it is the most likely subsurface release pathway of radionuclides to the LWB. WIPP PA calculations include a transient, dual-porosity mass transport model of the Culebra, last updated in the 2009 Performance Assessment Baseline Calculations (PABC-2009) with new flow calculations and updated transport parameters [3].

Radionuclide movement through the Culebra is a function of the groundwater flow-field and the transport properties of the radionuclide species being considered. Groundwater flow velocity and direction are highly dependent upon the magnitude and the spatial variability of hydraulic transmissivity (the T-field). WIPP PA considers the potential that future potash mining in the McNutt potash zone of the Salado Formation underlying the Rustler Formation will cause subsidence in the Culebra and hence increase Culebra hydraulic transmissivity.

Two types of uncertainty are considered in the WIPP PA, stochastic uncertainty and subjective uncertainty. WIPP PA addresses stochastic uncertainty in the Culebra transport simulations by defining a set of two mining scenarios and four radionuclide release points, and then employing a Monte Carlo analysis to randomly sample from across the set of possible futures. WIPP PA addresses subjective uncertainty by defining probability distributions for subjectively uncertain parameters. Latin Hypercube Sampling (LHS) is used to create 3 ensembles (replicates) of 100 distinct parameter sets (vectors) for a total of 300 separate realizations that are sampled across the range of parameter uncertainty. For most subjectively uncertain, spatially distributed quantities (e.g., Culebra fracture porosity), the sampled value of each realization is specified as a constant over the entire model domain.

The output of interest for WIPP PA are the cumulative mass flux to LWB of each simulated radionuclide, which are then convolved with releases to the Culebra to calculate radionuclide release from the Culebra. Releases from the Culebra have previously been a minor fraction of the total releases, including in the most recent compliance calculations in CRA19. However, releases to the Culebra can be significant, indicating the processes within the Culebra are an important component of the containment system. This paper aims to describe and quantify the important controls on Culebra transport from sources to the northwest of the existing waste panels.

BACKGROUND

The WIPP repository is located approximately 42 kilometers southeast of Carlsbad, New Mexico. The disposal horizon of the WIPP is approximately 655 meters below the ground surface in the Salado Formation of the Delaware Basin. The Salado is regionally extensive, consisting predominantly of halite, a low permeability evaporite [4].

The Rustler Formation is located stratigraphically above the Salado Formation and is of particular importance in estimating the potential for radionuclide releases from the WIPP because it contains the most hydraulically transmissive units above the repository. Near the WIPP, the Rustler consists of evaporite units interbedded with carbonates and siliciclastic units [5, 6]. The Culebra Dolomite Member has been identified as the most transmissive unit in the Rustler Formation and consequently it is the most likely pathway for subsurface transport of radionuclides from the WIPP panels to the accessible environment outside the LWB.

The Culebra is an approximately 7.75-meter-thick fractured dolomite with nonuniform properties in both the horizontal and vertical directions [7]. There are multiple scales of porosity and permeability within the Culebra ranging from microfractures to potentially large vuggy zones. Flow occurs through fractures, vugs and, to some extent, through intergranular pores. The large permeability contrast between the different scales of interconnected porosity suggests a dual porosity conceptualization consisting of advective porosity (i.e., fracture porosity) and diffusive porosity (i.e., matrix porosity). The advective porosity is the void space comprised of the highly transmissive portions of the rock such as large open fractures and/or interconnected vugs. The diffusional porosity represents the intragranular porosity potentially including microfractures or vugs. Tracer tests conducted in the Culebra at the WIPP site have shown characteristics of both advective transport and matrix diffusion [8].

Potash mining in the WIPP area involves resource extraction below the Culebra dolomite in the McNutt Potash zone, a subsection of the larger Salado Formation that underlies the Rustler Formation. It is hypothesized that subsidence of the Culebra due to potash mining leads to fracturing and unconsolidation, resulting in higher Culebra transmissivities. This increase in transmissivity may significantly change the regional groundwater flow pattern in the Culebra and additionally the transport of any nuclides entering the aquifer from the underlying repository. Mining scenarios include the full mining scenario in which mining occurs throughout the domain, and the partial mining scenario in which mining occurs only outside of the LWB.

The most recent update to the Culebra flow and transport calculations was made for the 2009 WIPP Performance Assessment Baseline Calculations (PABC09), as documented in [3]. Key findings from that report include that mass transported to the LWB was significantly higher in the full mining scenario than

the partial mining scenario, and higher for U-234 than the other isotopes, though all scenarios and isotopes achieved much less than complete breakthrough at the LWB. Conservative particle travel times to the LWB were also significantly lower in the full-mining scenario than the partial mining or no mining scenarios. A full sensitivity analysis on the mass transport results was not performed, but a correlation analysis indicated that the mining factor was not a strong control on conservative particle travel times [3].

The analysis presented in this paper is modeled after the PA Culebra transport compliance calculations from 2009 WIPP Performance Assessment Baseline Calculations (PABC09), with several important differences. Transport simulation times were increased from 10,000 years to 100,000 years to capture more complete breakthrough from relatively slow traveling radionuclides. The additional simulation time was added solely to yield a more complete picture of system behavior and has no relevance on the site compliance. Since the CCA, Culebra transport calculations considered only a single release point at the center of the 10-panel repository, referred to in this study as Culebra Release Point 1 (CRP1). Three additional Culebra release points (CRP2 through CRP4) were added over the additional panels region to assess the impact of the additional panels on WIPP PA calculations.

MODEL SETUP

Culebra transport simulations calculate the cumulative mass discharge of each radionuclide at the WIPP LWB in 50-year increments over the simulation period due to discrete sources (release points) located over the waste panel area. The key steps in estimating radionuclide transport through the Culebra include:

1. Construction of base geostatistical realizations of Culebra hydraulic transmissivity (T), anisotropy, storativity, and recharge fields (collectively referred to as "T-fields");
2. Calibration of the T-fields to observed heads;
3. Modification of the T-fields to account for potential mining-induced subsidence;
4. Calculation of steady-state groundwater flow-fields for each mining-modified T-field using the software MODFLOW-2000; and
5. Calculation of radionuclide transport through the Culebra for each flow-field using the WIPP PA transport software SECOTP2D.

The work reported herein includes modifications to Step 5 and a reanalysis of the results of Step 4 using additional release points to characterize transport emanating from sources to the west of the existing waste region. Figure 1 illustrates the modeling domains and other features of interest.

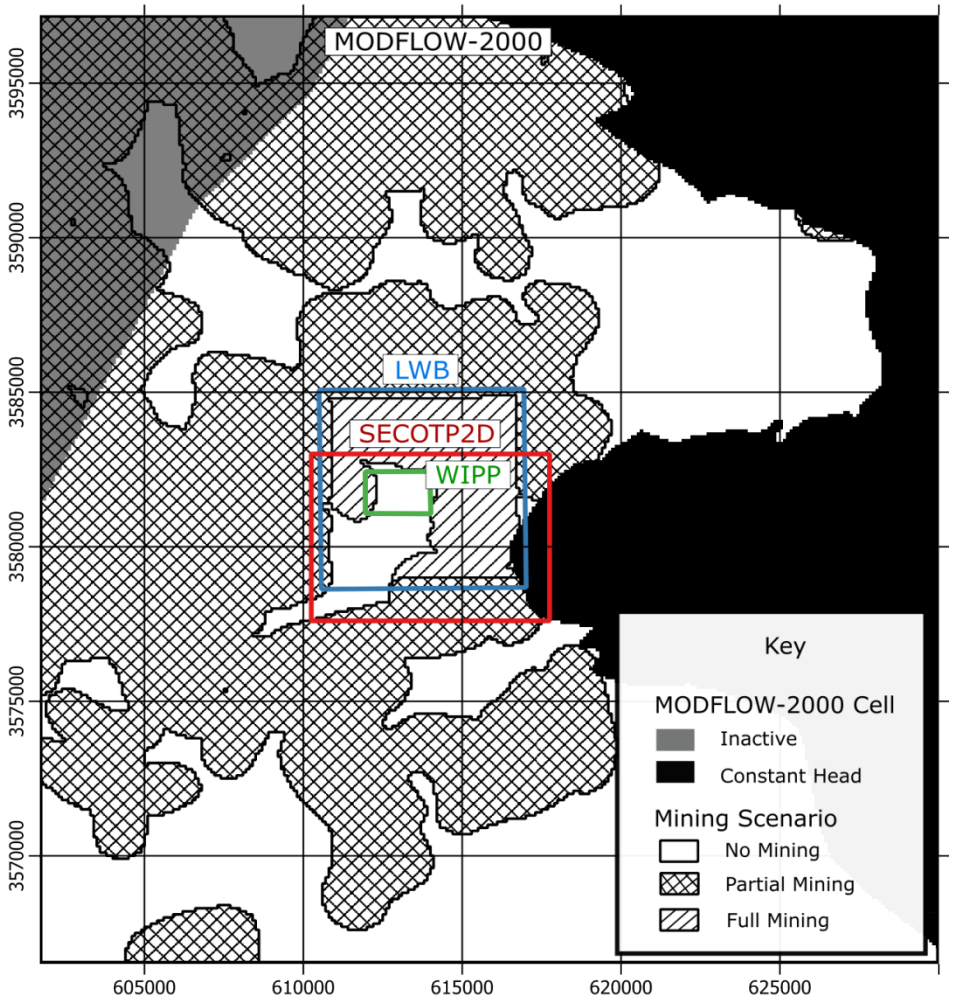

Figure 1. Culebra Modeling Domain

Steady-state Flow

Culebra flow fields from the 2009 WIPP Performance Assessment Baseline Calculations (PABC09) were used without modification. The Culebra is modeled as a single horizontal layer of uniform 7.75 m vertical thickness in MODFLOW-2000. The flow model domain is aligned with the primary compass directions and is aerially discretized into 100-m square cells, yielding a model that is 284 cells or 28.4 km in the east-west direction by 307 cells or 30.7 km in the north-south direction.

To simulate the effects of mining, the calibrated Culebra transmissivity values are multiplied by a random scaling factor (defined to be a subjectively uncertain parameter with a uniform distribution from 1 to 1000) in areas potentially impacted by mining. The steady-state flow model is then run with the modified

transmissivity to produce the mining-affected flow distributions for input to the transport model. Only the full mining results are presented in this analysis because of their greater impact on WIPP PA results (Figure 2).

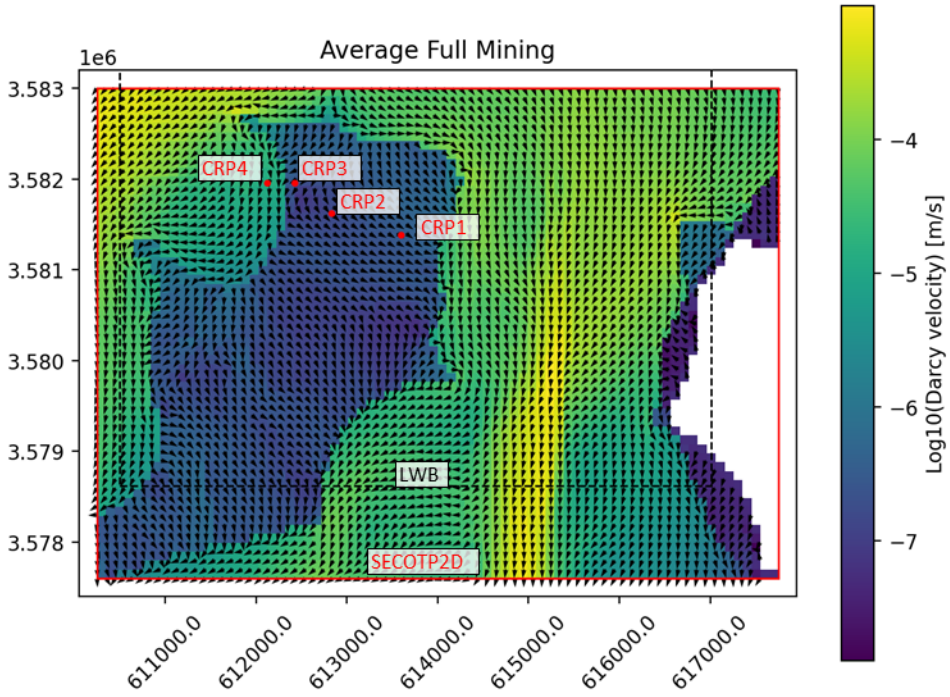

Figure 2. Average MODFLOW-2000 Darcy Velocity, Full Mining Scenario

Particle tracking calculations were performed using the WIPP software DTRKMF on the flow fields to visualize, quantify, and compare the particle travel characteristics from across the waste region, including the additional panels region, and then derive a set of four release points (CRP1 through CRP4) that encompass a representative range of advective travel time distributions to the LWB. The particle tracking results illustrate the advective pathway taken by a marked water particle, and do not take into consideration retardation, dispersion, or molecular diffusion. A single particle is tracked in each simulation.

Results are presented below for CRP1 and CRP4 particle tracks (Figure 3) and travel times to the LWB (Figure 4). CRP1 is coincident with the sole release point used in PABC09 simulations. CRP4 captures relatively fast traveling particles that travel to the west and exit the LWB relatively quickly in the full mining scenario. Travel times to the LWB are summarized in cumulative distribution function plots.

Consistent with the PABC09 [3], the travel times to the LWB had a slight positive correlation with the mining factor in CRP1 (Figure 5). In contrast, CRP4 shows a steep negative correlation to DTRKMF travel times at low mining factors and no or very low correlation at higher mining factors.

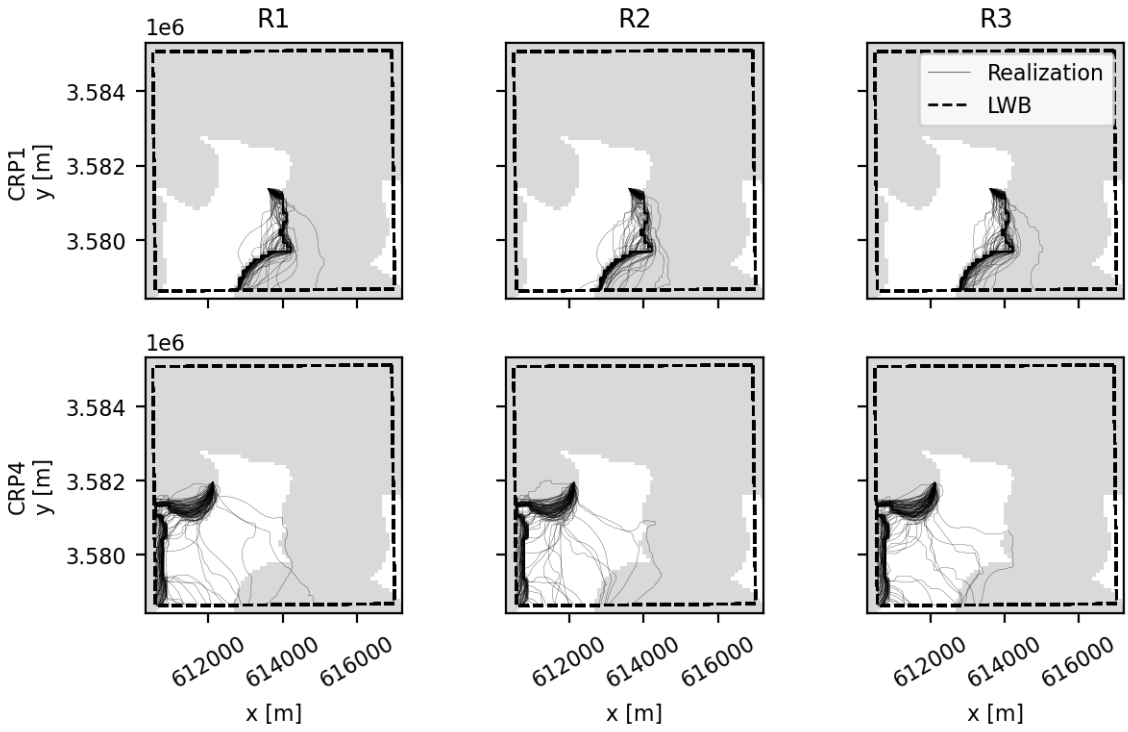

Figure 3. RPPA DTRKMF Travel Paths, Full Mining Scenario

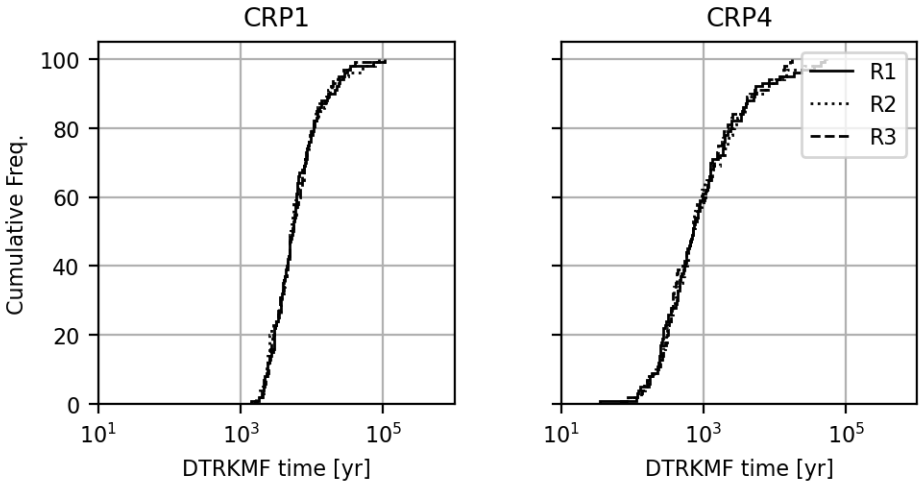

Figure 4. RPPA DTRKMF Travel Times to LWB, Full Mining Scenario

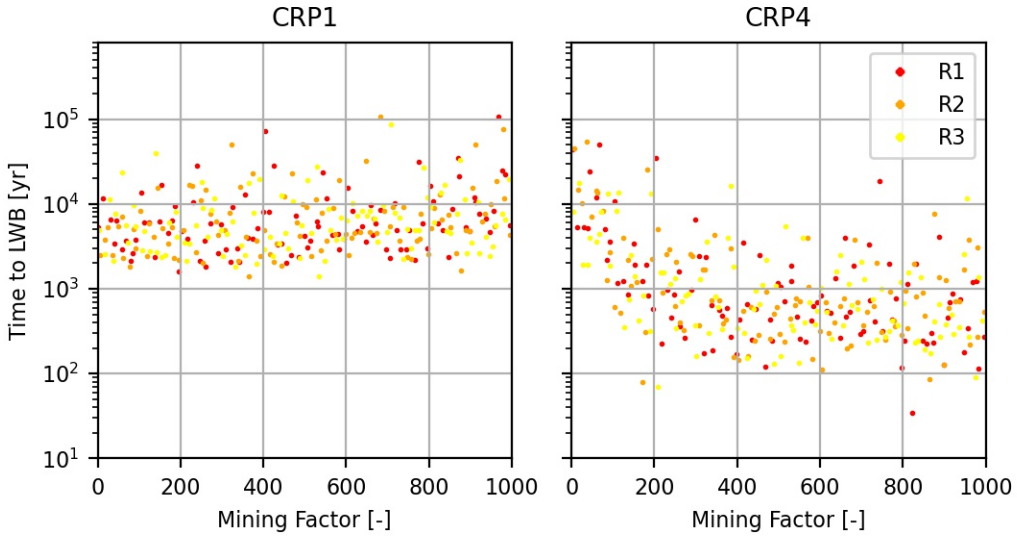

Figure 5. DTRKMF Travel time to LWB [yr] vs Mining Factor

Mass Transport

Transport simulations are calculated for each combination of mining scenario and release point using the WIPP PA transport software SECOTP2D. The Culebra transport computational grid is created by subdividing the Culebra flow model cells into equal-sized 50-m grid cells within a subregion over the WIPP region (Figure 1). The transport domain is approximately 7.5 km by 5.4 km, aligned with the principal compass directions and the principal directions of the groundwater flow domain. The transport domain extends beyond the LWB in the east-west direction and is shifted off-center such that it extends from a point midway between the center of the waste panels and the northern LWB to approximately 1 km beyond the southern edge of the LWB because the undisturbed groundwater flow direction is generally north to south.

The transport simulations assume parallel plate fracturing where fluid flow is restricted to the fracture domain, mass is transferred between the fracture and matrix domains via molecular diffusion, and retardation is restricted to the matrix domain. In each transport simulation, 1 kg of each of four radionuclides is released at one of the four release points during the first 50 years after repository closure. The radionuclides transported in the Culebra PA calculations are Am-241, U-234, Th-230, and Pu-239.

Mass transport in the fracture domain is governed by:

$$\phi R_l \frac{\partial C_l}{\partial t} = \nabla.(\phi D_l \nabla C_l - V C_l) - \phi R_l \lambda_l C_l + \phi R_{l-1} \lambda_{l-1} C_{l-1} + Q_l + \Gamma_l \quad (1)$$

where C_l is the unknown concentration of the lth radionuclide [kg/m^3], V is the specific discharge vector [m/s], D_l is the second-rank hydrodynamic dispersion tensor [m^2/s], ϕ is the dimensionless advective porosity, R_l is the dimensionless retardation coefficient, $\lambda_l$is the radioactive species decay constant [1/s],

Q_l is the specific injection rate [kg/(m³·s)], and Γ_l is the mass transfer coefficient between the advective and diffusive domains [kg/(m³·s)]. In WIPP PA calculations, only the concentration and mass transfer coefficients are both spatially and temporally variable. The velocity vector is spatially variable and steady state.

Mass transport in the diffusive domain is governed by:

$$\phi' R'_l \frac{\partial C'_l}{\partial t} - \frac{\partial}{\partial \chi}\left(\phi' D'_l \frac{\partial C'_l}{\partial \chi}\right) = -\phi' R'_l \lambda_l C'_l + \phi' R'_{l-1} \lambda_{l-1} C'_{l-1} \quad (2)$$

where χ is the spatial coordinate originating from the symmetry line of a matrix block [m], and D'_l is the matrix diffusion coefficient [m²/s]. All other symbols in Equation 2 have analogous meaning as Equation 1 for advective transport except that the prime denotes diffusive domain properties.

The advective and diffusive domains are coupled through the mass transfer term Γ_l, defined as:

$$\Gamma_l = -\frac{2\phi}{b}\left(\phi' D'_l \left.\frac{\partial C'_l}{\partial \chi}\right|_{\xi=B}\right) \quad (3)$$

where B is the matrix half-block length [m], b is the fracture aperture [m], and the term in the parentheses represents the mass flux per unit area of contact between the advective and diffusive continua. The term $2\phi/b$ represents the specific surface area (ratio of surface area to bulk volume) of the coupled system.

The retardation coefficient in the diffusive domain is defined by:

$$R'_l = 1 + \rho_s k_d^l \frac{(1-\phi')}{\phi'} \quad (4)$$

where ρ_s is the Culebra grain density and k_d^l is the distribution coefficient for species *l*. The retardation coefficient is set to 1 in the advective domain.

Input parameters and distributions are summarized in TABLE 1. Both longitudinal and transverse dispersivity coefficients are set to zero in WIPP PA calculations, resulting in a dispersion tensor that captures only molecular diffusion. WIPP PA treats advective and diffusive porosity, matrix half-block length, and the matrix distribution coefficients as subjectively uncertain (TABLE 1). Additional sampled parameters a random number used to select a flow realization for transport analysis (TRANSIDX), the climate index factor (CLIMIDX), and the oxidation state index (OXSTAT). The TRANSIDX parameter is used to create a random pairing between the mining impacted flow field and transport parameters. The CLIMIDX parameter is used to scale the mining-modified flow velocity to account for the potential impact of climate change [9]. The OXSTAT parameter is used to randomly determine simulation oxidation state, which is then used to select the appropriate matrix distribution coefficient k_d^l in the matrix retardation calculations. Two oxidate states are modeled in the PA simulations, each with equal 50% likelihood: lower oxidation with all Pu modeled as Pu(III) and all U modeled as U(IV), or higher oxidation with all Pu as Pu(IV) and all U as U(VI). Mixed oxidation states are not simulated.

TABLE 1. Input Parameter Ranges						
	Material: Property	**Units**	**Distribution**	**Minimum**	**Maximum**	**Median**
Longitudinal dispersivity	CULEBRA:DISPT_L	m	NA			0
Transverse dispersivity	CULEBRA:DISP_L	m	NA			0
Fracture tortuosity	CULEBRA:FTORT	-	NA			1
Matrix tortuosity	CULEBRA:DTORT	-	NA			0.11
Skin resistance	CULEBRA:SKIN_RES	-	NA			0
Material grain density	CULERBA:DNSGRAIN	kg/m^3	NA			2820
Advective porosity	CULEBRA:APOROS	-	log-uniform	1.00E-04	1.00E-02	1.03E-03
Diffusive porosity	CULEBRA:DPOROS	-	cumulative	1.00E-01	2.50E-01	1.60E-01
Matrix half-bock length	CULEBRA:HMBLKLT	m	uniform	5.00E-02	5.00E-01	2.75E-01
Climate index	GLOBAL:CLIMTIDX	-	cumulative	1.00E+00	2.25E+00	1.17E+00
Mining factor	CULEBRA: MINP_FAC	-	uniform	1.00E+00	1.00E+03	5.01E+05
Oxidation state	GLOBAL:OXSTAT	-	uniform	0.00E+00	1.00E+00	5.00E-01
Matrix distribution coefficient		-	-	-	-	-
Am(III)	AM+3:MKD_AM	m^3/kg	log-uniform	5.00E-03	4.00E-01	4.50E-02
Pu(III)	PU+3:MKD_PU	m^3/kg	log-uniform	5.00E-03	4.00E-01	4.50E-02
Pu(IV)	PU+4:MKD_PU	m^3/kg	log-uniform	5.00E-04	1.00E-01	7.10E-02
Th(IV)	TH+4:MKD_TH	m^3/kg	log-uniform	5.00E-04	1.00E-01	7.10E-02
U(IV)	U+4:MKD_U	m^3/kg	log-uniform	5.00E-04	1.00E-01	7.10E-02
U(VI)	U+6:MKD_U	m^3/kg	log-uniform	3.00E-05	2.00E-02	7.70E-04

Sensitivity Analysis

The STEPWISE PA software is used in a sensitivity analysis to determine the relative importance of the input variables in the Culebra transport calculations through a stepwise ranked regression analysis. Sampled input parameter values are input into STEPWISE as the independent variables together with the DTRKMF travel times to the LWB as an integrated metric of the underlying flow field. Sampled OXSTAT parameter values were used to derive a single ensemble of matrix distribution coefficients for each of Pu and U consistent with the simulation inputs that are used as independent regression variables. Dependent variables include the SECOTP2D Culebra mass transport to the LWB output.

Output reported by STEPWISE include standardized regression coefficients (SRCs) of the independent and dependent variables and the coefficients of determination (R^2). The variables in the SRC calculations are standardized by subtracting the variable mean and scaling by the variable standard deviation. The SRC varies between -1 and 1, with -1 indicating a perfectly negative correlation and 1 indicating a perfectly positive correlation. The R^2 value measures the fraction of the variation in the dependent variable attributable to the regression on the independent variable. The R^2 value varies between 0 and 1, with 0 indicating no relationship and 1 indicating a perfect relationship.

RESULTS

Results are presented for the full mining scenario, CRP1 and CRP4 simulations, and U-234 and Pu-239 isotopes (Figure 5). Horsetail plots show the cumulative release at the LWB over the 100,000-year simulation period. Mass released to the LWB is shown in terms of cumulative histograms of mass reaching the LWB by t=10,000 years and t=100,000 years model time, and cumulative histograms of the mean breakthrough time. Mean breakthrough time is normalized by the total mass transported to the LWB over

100,000 years such that it represents the mean breakthrough time of mass that did reach the LWB. The horsetail plots show only the 100 simulations from Replicate 1, while the three sets of summary histogram plots show all three replicates of 100 simulations each.

Several features are apparent in the plotted data. Mass breakthrough at the LWB from CRP4 is more frequent, more complete, and happens on average earlier than mass released into CRP1 for both U-234 and Pu-239. As expected, the releases at 100,000 years are greater than the releases at 10,000 years across the distribution of results for all scenarios, but even at 100,000 years run-time many simulations show little breakthrough at the LWB, particularly in CRP1 and Pu-239. The mass transport horsetails and inflection points in the mean breakthrough times both indicate that many simulations show significant breakthrough relatively early in the simulation before plateauing, while relatively few simulations continue to show appreciable breakthrough at later model times. Because the mean breakthrough times are normalized to the total breakthrough at 100,000 years, they may be affected by numerical noise in the extremely low release simulations. All scenarios show a significant proportion of simulations with less than 1e-10 kg total breakthrough at 100,000 years, ranging from approximately 10% of the CRP4, U-234 output to approximately 50% of the CRP1, Pu-239 output, with the other simulation output in between.

Sensitivity Analysis

A subset of the SECOTP2D output associated with the CRP1 and CRP4 release points and full-mining scenarios was selected for sensitivity analysis with STEPWISE.

Dependent variables include Pu-239 and U-234 cumulative mass flux output and mean release time output. Independent variables include DTRKMF-predicted particle travel times to the LWB, as an integrated measure of the flow velocity field (identified as DTRKMF in the results tables below), the climate index multiplier [CLIMIDX], the dual porosity transport parameters fracture porosity [FPOROS], matrix porosity [MPOROS], half matrix block length [HMBLKLT], and the matrix distribution coefficient [CMKDU, CMKDPU] sampled for each isotope at the randomly selected oxidation state.

The STEPWISE output correlations indicate that matrix distribution coefficients and DTRKMF travel times are consistently the input most strongly associated with variation in mass transport to the LWB at 10,000 years and 100,000 years (TABLE 2, TABLE 3). Matrix retardation was more strongly associated with all metrics of U-234 mass transport than Pu-239. The negative correlation indicates that lower matrix distribution coefficients are associated with larger releases, as expected. The rank correlations with DTRKMF travel times were stronger for CRP4 than CRP1 and stronger for Pu-239 than U-234. The negative correlation indicates that shorter travel times are associated with larger releases, again, as expected. Correlations with the 10,000-year fluxes are generally weaker than those for the 100,000-yr fluxes, particularly for Pu-239, likely because of the greater number of simulations with extremely low breakthrough. Other parameters identified in the correlation analysis include the climate factor and several dual-porosity parameters, including fracture porosity and half matrix block length. However, the impact of these parameters is small relative to both matrix distribution coefficient and the DTKRMF travel times.

The STEPWISE output correlations for the mean breakthrough time dependent variables were weaker and more variable (TABLE 4). Fracture porosity more consistently appears as a controlling input, particularly in CRP1 simulations, along with the matrix distribution coefficients, and DTRKMF travel times.

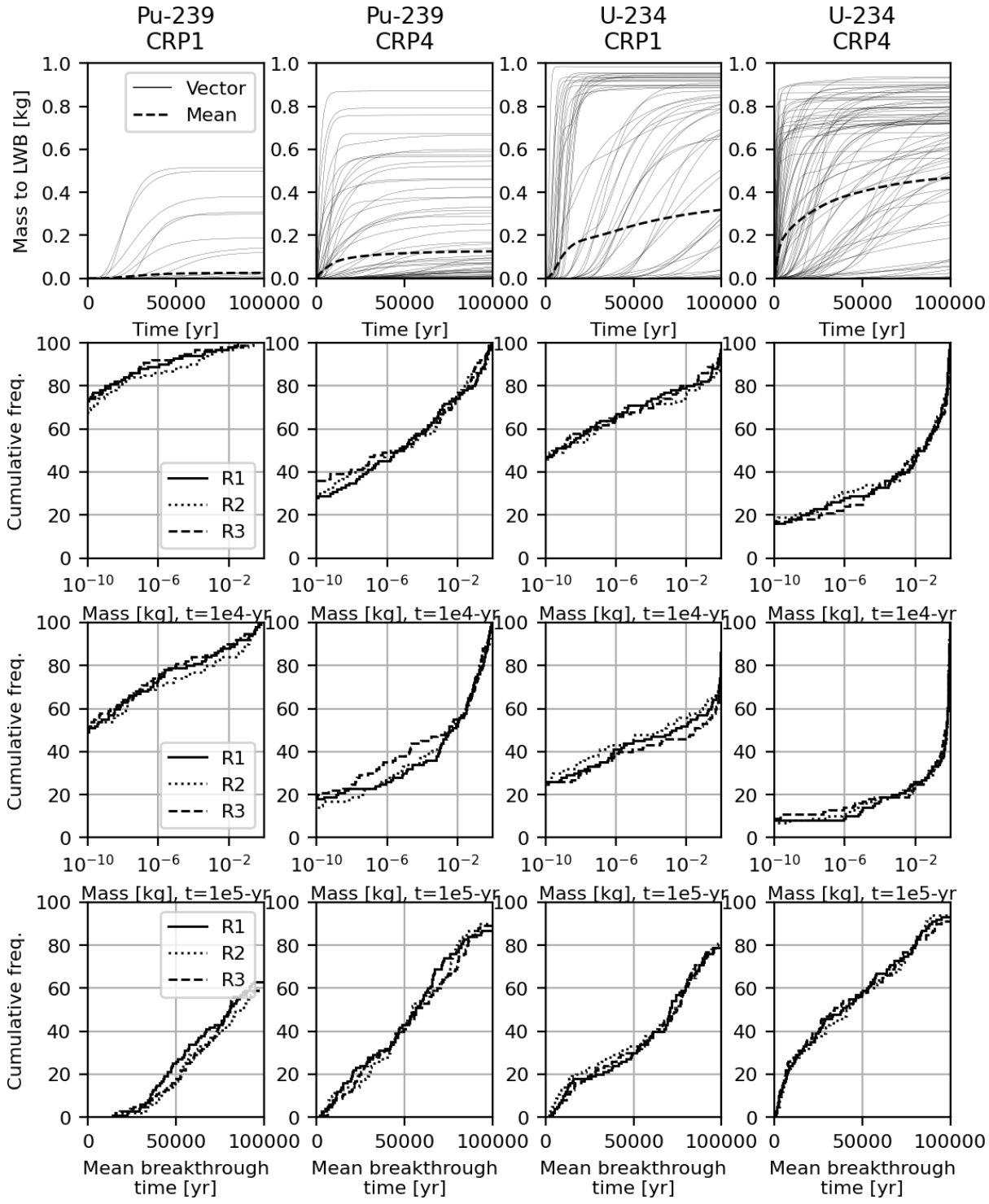

Figure 5. Culebra Transport to the LWB Results, Full Mining

TABLE 2. Ranked Regression Output, Cumulative Release (t=10,000-yrs)

	U-234						Pu-239					
Replicate 1	CRP1			CRP4			CRP1			CRP4		
Step	Variable	R^2	SRC	Variable	R^2	SRC	Variable	R^2	SRC	Variable	R^2	SRC
1	CMKDU	0.71	-0.86	CMKDU	0.63	-0.82	CMKDPU	0.33	-0.63	CMKDPU	0.41	-0.61
2	APOROS	0.75	-0.21	DTRKMF	0.86	-0.49	HMBLKLT	0.47	0.38	DTRKMF	0.72	-0.58
3	DTRKMF	0.78	-0.17	APOROS	0.87	-0.08	APOROS	0.54	-0.28	HMBLKLT	0.75	0.15
Replicate 2	CRP1			CRP4			CRP1			CRP4		
Step	Variable	R^2	SRC	Variable	R^2	SRC	Variable	R^2	SRC	Variable	R^2	SRC
1	CMKDU	0.70	-0.86	CMKDU	0.66	-0.86	CMKDPU	0.35	-0.55	CMKDPU	0.42	-0.60
2	DTRKMF	0.77	-0.27	DTRKMF	0.82	-0.39	HMBLKLT	0.40	0.23	DTRKMF	0.65	-0.49
3	APOROS	0.79	-0.14	HMBLKLT	0.84	0.14	--	- -	--	HMBLKLT	0.72	0.25
Replicate 3	CRP1			CRP4			CRP1			CRP4		
Step	Variable	R^2	SRC	Variable	R^2	SRC	Variable	R^2	SRC	Variable	R^2	SRC
1	CMKDU	0.63	-0.80	CMKDU	0.69	-0.85	CMKDPU	0.27	-0.53	CMKDPU	0.41	-0.69
2	DTRKMF	0.72	-0.28	DTRKMF	0.87	-0.42	DTRKMF	0.35	-0.28	DTRKMF	0.73	-0.55
3	APOROS	0.76	-0.21	CLIMTIDX	0.88	0.09	APOROS	0.38	-0.17	CLIMTIDX	0.76	0.19

TABLE 3. Ranked Regression Output, Cumulative Release (t=100,000-yrs)

	U-234						Pu-239					
Replicate 1	CRP1			CRP4			CRP1			CRP4		
Step	Variable	R^2	SRC	Variable	R^2	SRC	Variable	R^2	SRC	Variable	R^2	SRC
1	CMKDU	0.84	-0.92	CMKDU	0.61	-0.79	CMKDPU	0.52	-0.79	CMKDPU	0.55	-0.71
2	DTRKMF	0.90	-0.27	DTRKMF	0.78	-0.42	DTRKMF	0.60	-0.31	DTRKMF	0.83	-0.53
3	CLIMTIDX	0.91	0.08	--	--	- -	HMBLKLT	0.68	0.29	CLIMTIDX	0.84	0.13
Replicate 2	CRP1			CRP4			CRP1			CRP4		
Step	Variable	R^2	SRC	Variable	R^2	SRC	Variable	R^2	SRC	Variable	R^2	SRC
1	CMKDU	0.81	-0.91	CMKDU	0.71	-0.88	CMKDPU	0.47	-0.62	CMKDPU	0.53	-0.69
2	DTRKMF	0.88	-0.28	DTRKMF	0.80	-0.30	DTRKMF	0.59	-0.35	DTRKMF	0.77	-0.48
3	APOROS	0.89	-0.07	--	--	--	HMBLKLT	0.64	0.23	HMBLKLT	0.81	0.21
Replicate 3	CRP1			CRP4			CRP1			CRP4		
Step	Variable	R^2	SRC	Variable	R^2	SRC	Variable	R^2	SRC	Variable	R^2	SRC
1	CMKDU	0.87	-0.95	CMKDU	0.73	-0.88	CMKDPU	0.48	-0.73	CMKDPU	0.49	-0.74
2	DTRKMF	0.92	-0.21	DTRKMF	0.83	-0.31	DTRKMF	0.62	-0.39	DTRKMF	0.79	-0.53
3	CLIMTIDX	0.93	0.09	HMBLKLT	0.85	-0.14	APOROS	0.70	-0.27	CLIMTIDX	0.81	0.14

TABLE 4. Ranked Regression Output, Mean Release Time

	U-234						Pu-239					
Replicate 1	CRP1			CRP4			CRP1			CRP4		
Step	Variable	R^2	SRC	Variable	R^2	SRC	Variable	R^2	SRC	Variable	R^2	SRC
1	CMKDU	0.60	0.79	CMKDU	0.67	0.83	CMKDPU	0.15	0.44	CMKDPU	0.33	0.54
2	APOROS	0.64	0.18	DTRKMF	0.89	0.47	APOROS	0.28	0.36	DTRKMF	0.59	0.52
3	HMBLKLT	0.66	-0.15	--	--	--	HMBLKLT	0.39	-0.34	HMBLKLT	0.64	-0.23
Replicate 2	CRP1			CRP4			CRP1			CRP4		
Step	Variable	R^2	SRC	Variable	R^2	SRC	Variable	R^2	SRC	Variable	R^2	SRC
1	CMKDU	0.54	0.78	CMKDU	0.70	0.88	CMKDPU	0.19	0.38	CMKDPU	0.32	0.50
2	DTRKMF	0.63	0.29	DTRKMF	0.85	0.39	APOROS	0.30	0.34	DTRKMF	0.52	0.44
3	APOROS	0.66	0.17	HMBLKLT	0.86	-0.12	HMBLKLT	0.39	-0.30	HMBLKLT	0.63	-0.33
Replicate 3	CRP1			CRP4			CRP1			CRP4		
Step	Variable	R^2	SRC	Variable	R^2	SRC	Variable	R^2	SRC	Variable	R^2	SRC
1	CMKDU	0.64	0.81	CMKDU	0.74	0.88	APOROS	0.20	0.45	DTRKMF	0.29	0.55
2	DTRKMF	0.70	0.23	DTRKMF	0.89	0.38	CMKDPU	0.34	0.38	CMKDPU	0.61	0.57
3	APOROS	0.75	0.23	CLIMTIDX	0.90	-0.08	--	--	--	DPOROS	0.65	0.18

DISCUSSION

The results indicate that mass released into the full-mining scenario, CRP4 release point results in earlier, more complete, and more frequent U-234 and Pu-239 breakthrough. Particles released at CRP4 travel relatively quickly to the western delineation of the WIPP LWB in full-mining simulations.

Mass transport after 10,000 years has no regulatory significance, but in this study the simulations were run out to 100,000 years to achieve stronger breakthrough and generate a more robust dataset for correlation analysis. In general, the 100,000-year cumulative mass transport output did produce stronger correlations, but in both the 10,000-year and 100,000-year output the controls are the oxidation state dependent matrix distribution factor and the DTRKMF travel times, with DTRKMF travel more strongly associated with the Pu-239 mass transport in CRP4 simulations. The larger range and lower values of the U-234 matrix distribution parameter give it more importance to the resulting mass transport relative to Pu-239, with less sensitivity to the input flow fields. In effect, mass reaches the LWB in simulations sampling from at the low range of the U-234 matrix distribution coefficient regardless of the input flow field.

Mean breakthrough time controls were explored, but correlations with the input parameters were moderate to weak. The total mass breakthrough may have been too low in too many simulations to produce meaningful mean breakthrough times. The simulations that did achieve majority breakthrough, CRP4 U-234, show strong controls of matrix distribution coefficients and DTRKMF travel times, consistent with the other metrics.

CONCLUSIONS

Culebra transport calculations are presented for isotopes Pu-239 and U-234 for the full mining scenario and two of four release points. The release points include the original release point (CRP1) over the existing waste panels and the westernmost release point (CRP4) over the proposed waste panels region. Mass breakthrough during the 10,000-year regulatory period was higher in the CRP4 simulations for both Pu-239 and U-234. The matrix distribution coefficient remains the most important control on mass transport. However, relative to CRP1, the DTRKMF travel times of CRP4 were more strongly associated with mass transport to the LWB. This result suggests that the Culebra flow calculations would take on increased importance for future PAs that include the additional panels. All associated files for this analysis are archived on the Sandia computing cluster FWM at /data/cvs/CVSLIB/WIPP_EXTERNAL/RPPA_Culebra/Files

REFERENCES

1. U.S. Congress. 1992. Waste Isolation Pilot Plant Land Withdrawal Act. ERMS 239105. Public Law 102-579, October 1992. 102nd Congress, Washington, DC.
2. U.S. Department of Energy (DOE). 1981. Consultation and Cooperation Agreement. U.S. Department of Energy Waste Isolation Pilot Plant, Carlsbad Field Office. Carlsbad, NM.
3. Kuhlman, K. 2010. Analysis Report for the CRA-2009 PABC Culebra Flow and Transport Calculations. Carlsbad, NM: Sandia National Laboratories. ERMS #552951
4. Powers, D.W., Lambert, S.J., Shaffer, S.-E., Hill, L.R. and Weart, W.D., eds., 1978. Geological Characterization Report- (WIPP). Carlsbad, NM: Sandia National Laboratories. SAND78-1596.
5. Vine, J.D., 1963. Surface Geology of the Nash Draw Quadrangle, Eddy County, New Mexico. U.S. Geological Survey. Bulletin 1141-B.
6. Holt, R.M. and Powers, D.W., 1988. Facies Variability and Post-Depositional Alteration Within the Rustler Formation in the Vicinity of the Waste Isolation Pilot Plant, Southeastern New Mexico. Carlsbad, NM: WIPP Project Office. ERMS #242145.
7. Holt, R.M., 1997. Conceptual Model for Transport Processes in the Culebra Dolomite Member of the Rustler Formation. Carlsbad, NM: Sandia National laboratories. SAND97-0194.
8. Meigs, L.C., Beauheim, R.L. and Jones, T.L., eds., 2000. Interpretation of Tracer Tests Performed in the Culebra Dolomite at the Waste Isolation Pilot Plant Site. Carlsbad, NM: Sandia National Laboratories. SAND97-3109.
9. Corbet, T. and Swift, P., 1996. Parameters required for SECOFL2D: Climate Index. Carlsbad, NM: Sandia National Laboratories. ERMS #237465.

ACKNOWLEDGEMENTS

Sandia National Laboratories is a multimission laboratory managed and operated by National Technology and Engineering Solutions of Sandia, LLC., a wholly owned subsidiary of Honeywell International, Inc., for the U.S. Department of Energy's National Nuclear Security Administration under contract DE-NA-0003525. This research is funded by WIPP programs administered by the Office of Environmental Management (EM) of the U.S. Department of Energy. SAND2022-11483A